Title

Deposition of nanometer-thick amorphous carbon films by filtered cathodic vacuum arc under oblique ion incidence conditions

Authors

Zhang, Hanshen

Komvopoulos, Kyriakos

Publication Date

2023-11-01

DOI

10.1016/j.tsf.2023.140045

Thin Solid Films 784 (2023) 140045

Contents lists available at ScienceDirect

Thin Solid Films

journal homepage: www.elsevier.com/locate/tsf

Deposition of nanometer-thick amorphous carbon films by filtered cathodic vacuum arc under oblique ion incidence conditions

Hanshen Zhang , Kyriakos Komvopoulos *

Department of Mechanical Engineering, University of California, Berkeley, CA 94720, USA

ARTICLE INFO

Keywords:
Amorphous carbon
Atom hybridization
Filtered cathodic vacuum arc
Ion incidence angle
Structure
Substrate bias voltage
Ultrathin films

ABSTRACT

Filtered cathodic vacuum arc (FCVA) is a promising technique for synthesizing extremely thin carbon films exhibiting highly tetrahedral (sp^3) carbon atom hybridization. However, most FCVA studies are for incident ions impinging perpendicular to the substrate surface. In this study, the effects of the ion incidence angle on the thickness, structure, and surface roughness of amorphous carbon (*a*-C) films deposited under different substrate bias voltages were examined in the light of computational and experimental results. Dynamic simulations and film thickness measurements showed a decrease in film thickness with increasing ion incidence angle, attributed to the decrease in carbon ion fluence on the film surface. Carbon atom hybridization analysis revealed a critical ion incidence angle for a given substrate bias voltage. Simulation and experimental results demonstrated that the enhancement of sp^3 hybridization resulted from carbon-carbon collision cascades on the growing film surface and densification induced by direct and recoil implantation processes controlled by the ion incidence angle and substrate bias voltage. The strong dependence of *a*-C film growth on the carbon ion incidence angle exemplified by the results of this study has direct implications in the oblique deposition of ultrathin *a*-C films with predominant tetrahedral carbon atom hybridization. The present study provides a framework for optimizing the ion incidence angle to achieve the deposition of *a*-C ultrathin films with high sp^3 contents.

1. Introduction

Tetrahedral (sp^3) carbon atom hybridization in amorphous carbon (*a*-C) films is the primary reason for the exceptional mechanical properties displayed by these films [1–3], making them ideal protective overcoats for numerous applications where preserving the surface integrity is critical to the device functionality and longevity. In particular, high demands for thin-film materials in leading-edge technologies, such as semiconductors, photodiodes, solar cells, miniaturized electromechanical systems, and magnetic storage devices, have generated increased interest in the development of *a*-C thin films displaying uniformity, ultralow surface roughness, and high hardness.

Among various thin-film deposition methods [4], filtered cathodic vacuum arc (FCVA) is a particularly effective technique for depositing continuous, highly tetrahedral, ultrathin films with excellent mechanical properties [1–7]. An intrinsic feature of FCVA is the development of a plasma comprising energetic ions (e.g., ~20 eV kinetic energy for C^+ ions [8]), which can be accelerated by applying a negative bias voltage to the substrate. Noteworthy developments of the FCVA technique aimed to achieve plasma stability and improved efficiency [9–16] led to the growth of *a*-C films demonstrating good thermal stability [17–19] and exceptional mechanical [11,20,21], tribological [22], and anti-oxidation [23,24] characteristics.

Film deposition by FCVA is a multi-parameter process. Earlier experimental and analytical studies illuminated important effects of key process parameters on the thickness and structure (i.e., type of hybridization) of *a*-C films. For example, *a*-C ultrathin films with 50–60 % sp^3 contents were synthesized by FCVA using substrate pulse bias voltages in the range of –25 to –100 V and ion incidence angle equal to 10° measured from the substrate normal [25]. The duty cycle of substrate pulse biasing can also affect the thickness, structure, and surface roughness of FCVA-deposited *a*-C films [26]. Molecular dynamics (MD) simulations showed that a C^+ ion kinetic energy of 80 eV produced *a*-C films with the highest density (3.3 g/cm^3) and sp^3 content (~43 %) [27], consistent with the classical subplantation model encompassing the simultaneously occurring processes of shallow subsurface implantation of energetic ions, preferential displacement of atoms with a low displacement energy, and sputtering of weakly bonded atoms [28–30].

* Corresponding author.
E-mail address: kyriakos@me.berkeley.edu (K. Komvopoulos).

https://doi.org/10.1016/j.tsf.2023.140045
Received 20 April 2023; Received in revised form 7 September 2023; Accepted 8 September 2023
Available online 9 September 2023

Moreover, MD simulations indicated the existence of a critical ion kinetic energy for growing *a*-C films with the highest sp^3 content and confirmed that film deposition processes that use energetic particles as film precursors, such as the FCVA method, produce *a*-C films with a layered structure consisting of an interfacial (intermixing) layer, a bulk layer rich in sp^3 hybridization, and a principally sp^2 hybridized surface layer [31], consistent with the findings of experimental investigations [32,33]. The foregoing studies indicated a strong effect of direct process parameters (e.g., ion incidence angle and substrate bias voltage) and indirect process parameters (e.g., ion kinetic energy and ion fluence) of the FCVA method on the resulting thickness, structure, and mechanical properties of *a*-C thin films.

Despite significant progress in film deposition using the FCVA process, in the majority of the film deposition experiments the energetic ions impinged perpendicular to the substrate surface and, subsequently, onto the surface of the growing film. However, in applications involving film deposition on patterned surfaces, the directionality of the plasma beam may vary significantly. This is mainly the case in applications necessitating ultrathin film deposition on miniaturized structures fabricated on a substrate surface, as illustrated schematically in Fig. 1. Particularly, the mechanisms controlling thin-film synthesis by an oblique incidence plasma beam may differ from those encountered under film growth conditions of normal ion incidence, subsequently affecting the quality of the grown film. Therefore, oblique FCVA film deposition requires more in-depth examination.

The main objective of this study was to investigate the effect of the ion incidence angle on the thickness, structure, and surface roughness of *a*-C thin films synthesized by FCVA at different substrate bias voltages. Results from dynamic simulations, X-ray photoelectron spectroscopy (XPS), surface profilometry, and atomic force microscopy (AFM) studies are presented below to illuminate the effect of the ion incidence angle on the carbon depth profile, sputtering yield, type of hybridization, thickness, and surface roughness of FCVA-deposited nanometer-thick *a*-C films. The obtained results provide insight into the deposition of ultrathin *a*-C films under oblique ion incidence FCVA conditions and an effective approach for optimizing the ion incidence angle at various substrate bias voltages for accomplishing the growth of highly sp^3 hybridized *a*-C films.

2. Methods

2.1. Deposition of carbon films

A custom-made direct-current FCVA system, described in detail elsewhere [16], was used to deposit *a*-C films on segments of a commercially available p-type Si(100) wafer with a root-mean-square (rms) surface roughness equal to ~0.2 nm. In all the FCVA experiments, the potential and current applied between the anode and the cathode were fixed at 24 V and 70 A, respectively, the C^+ ion flux at normal incidence (i.e., zero incidence angle) was set equal to ~1.5 × 10^{15} ions/cm^2·s, and the deposition time was fixed at 1 min (i.e., C^+ ion fluence at normal incidence equal to ~9 × 10^{16} ions/cm^2). The kinetic energy of the C^+ ions in the plasma cloud was ~20 eV [8]. The Si substrate was affixed to the center of the sample holder, which was biased by a time-average voltage of –25 or –50 V, applied at a pulse frequency of 25 kHz. A typical waveform of the substrate pulse bias voltage is shown in Fig. 2.

Oblique plasma beam incidence is schematically depicted in Fig. 3a. The incidence angle is defined as the angle between the trajectory of the plasma beam and the normal to the substrate surface. The positively charged ions of the plasma accelerated through the electric sheath surrounding the negatively biased substrate. Accordingly, the electric

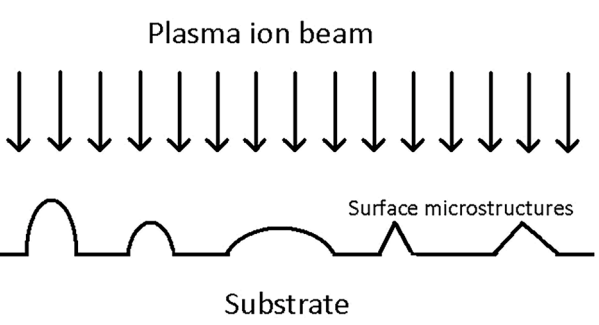

Fig. 1. Schematic illustration of a plasma beam interacting with a patterned solid surface. The various geometric features at the surface result in locally oblique incidence of the impinging plasma ions.

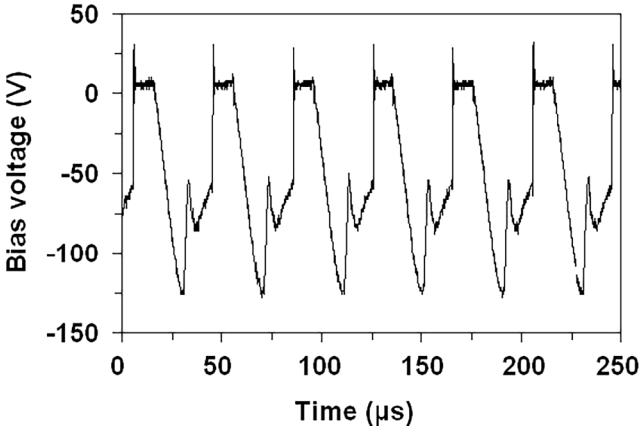

Fig. 2. Waveform of a pulse substrate bias voltage with –50 V time-average magnitude and 25 kHz frequency.

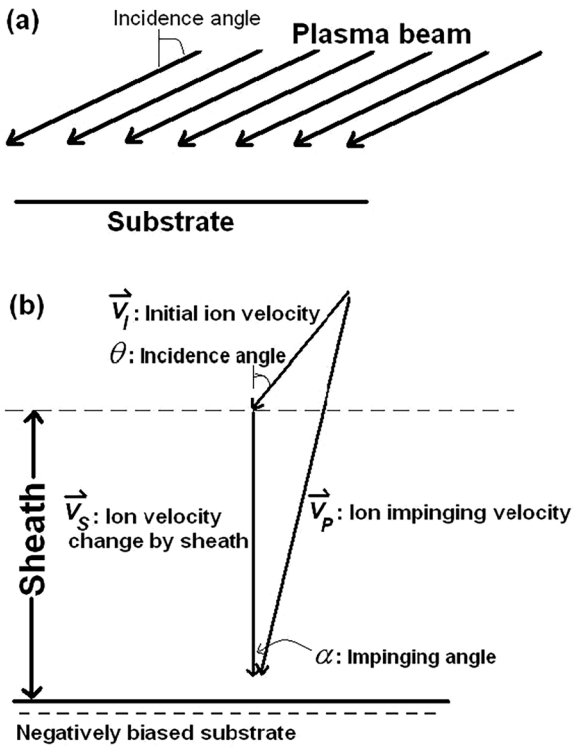

Fig. 3. (a) Plasma-surface interaction at ion incidence angle θ and (b) schematic illustration of the change in initial ion velocity V_I and ion incidence angle θ to ion impinging velocity V_P and ion impinging angle α due to the velocity V_S introduced by the electric sheath produced at the substrate surface by the applied negative bias voltage.

sheath increased the ion kinetic energy, while changing the magnitude and trajectory of the initial ion velocity V_I, resulting in ion impinging angle α smaller than the ion incidence angle θ and ion impinging velocity V_P greater than V_I (Fig. 3b). Because ion acceleration due to substrate pulse biasing commenced perpendicular to the substrate surface, the magnitude of the bias voltage controlled both the ion kinetic energy and the ion impinging angle.

Before the actual experiments, some preliminary depositions were performed at ion incidence angles in the range of 40–70° without rotating the substrate. The objective of these experiments was to examine whether oblique ion incidence deposition could yield anisotropic surface features, as previously observed for considerably higher ion bombarding energy [34]. For the highest substrate bias voltage applied in the present depositions (i.e., –50 V), the resulting FCVA process conditions did not produce any surface anisotropies. Nevertheless, to obtain films of uniform thickness, in all film depositions the substrate was rotated at a constant speed of 60 rpm.

A mechanical stylus profilometer (Dektak 3030 profiler, Veeco Instruments, Plainview, NY) with 0.1 nm height resolution (12.5 μm stylus radius, 25 mg stylus force, and ≥50 μm scan length) was used to measure the film thickness. This was accomplished by traversing the lightly loaded stylus tip perpendicular to the boundary of coated and uncoated (covered with a Si piece) surface regions in each sample.

2.2. Simulations

Film growth was simulated with the T-DYN software (version 4.0), a dynamic simulation code based on the TRIM code [35–40], which has been verified by experimental results of atomic mixing [41], depth profiles [28,29,42,43], and sputter yield [44,45]. Details of the conditions and algorithms can be found elsewhere [41,43]. The binding energies of Si and C were set equal to 2.32 and 2.27 eV, respectively, whereas the corresponding surface binding energies were assumed to be equal to 4.7 and 7.41 eV, respectively. These binding energy values are typical of solid-state silicon and graphite.

2.3. Structure and surface roughness analysis

The effects of the ion incidence angle and substrate pulse biasing on the structure (i.e., carbon atom hybridization) of the *a*-C films were systematically studied by XPS. This technique provides quantitative information about the bonding energy and percentages of different atomic carbon hybridizations, in conjunction with relevant information about high-energy contamination bondings [46,47]. The deposited *a*-C films were characterized with an XPS system (PHI 5400, Physical Electronics, Chanhassen, MN) equipped with a monochromatic X-ray source of Al-Kα (1486.6 eV photon energy). The spectrometer was operated at a pass energy of 35.75 eV for the C1s window scan. A 0.05 eV energy step applied in increments of 50 ms was used to acquire the XPS spectra of the C1s core-level peak. The pressure in the XPS analyzing vacuum chamber was maintained below 2.67×10^{-6} Pa. The samples were not sputter cleaned before the XPS analysis.

The rms surface roughness of the *a*-C films was measured with an AFM setup (Dimension 3100, Veeco Instruments, Plainview, NY), using a 1×1 μm^2 scan area. The AFM was operated in tapping mode at 259.332 kHz drive frequency and 2 Hz scan rate.

3. Results and discussion

A model of the ion incidence onto the substrate surface was developed for the T-DYN simulations. The ion fluence on the substrate surface was calculated by multiplying the ion fluence normal to the surface (i.e., $\sim9 \times 10^{16}$ ions/cm^2) by the cosine of the ion incidence angle (Fig. 3b). The electric sheath due to substrate pulse biasing changed the velocity of the impinging ions, consequently changing the kinetic energy of the bombarding C^+ ions. The change in ion kinetic energy was controlled by the substrate bias voltage, not by the ion incidence angle. For example, for a –50 V time-average bias voltage and ~20 eV initial ion kinetic energy, the kinetic energy of the C^+ ions impinging onto the substrate surface was equal to ~70 eV, regardless of the ion incidence angle. However, the ion impinging angle was affected by both the ion incidence angle and the magnitude of the substrate bias voltage. The direct and indirect process parameters, including the change in ion velocity V_S and the impinging angle (Fig. 3b), are related through the following relations:

$$E_P = E_I + E_S$$

$$E_I = \frac{1}{2} m_C V_I^2$$

$$E_P = \frac{1}{2} m_C V_P^2$$

$$V_P^2 = (V_I \sin\theta)^2 + (V_I \cos\theta + V_S)^2$$

$$\frac{V_I \sin\theta}{V_I \cos\theta + V_S} = \tan\alpha$$

$$\Phi_P = \Phi_I \cos\theta$$

where E_P is the kinetic energy of the ions impinging onto the substrate surface, E_I is the initial ion kinetic energy (~20 eV), E_S is the change in ion kinetic energy caused by the electric sheath (substrate bias voltage), m_C is the mass of a carbon ion (1.994×10^{-23} g), and Φ_I and Φ_P are the initial ion incidence fluence and the ion fluence on the substrate surface, respectively. Calculated values of V_S and α for –25 and –50 V substrate bias voltages are given in Table 1. These data were input in the T-DYN simulations of the carbon depth profiles.

Fig. 4 shows carbon depth profiles in a Si substrate simulated with the T-DYN code for ion incidence angles in the range of 0–80°. In all simulation cases, the *a*-C film thickness decreased with the increase of the ion incidence angle due to the decrease of the ion fluence (Table 1). Moreover, the increase of the substrate bias voltage enhanced Si-C intermixing. This is evinced by comparing the depth range with atomic carbon <100 %, for a given ion incidence angle. The enhancement of Si-C intermixing was attributed to the intensified direct and recoil implantation caused by the increase of the ion kinetic energy. Thus, the film thickness strongly depended on the substrate bias voltage (ion kinetic energy) and the ion incidence angle.

A comparison of the *a*-C film thickness values obtained from the T-DYN simulations (Fig. 4) with experimentally measured values (Fig. 5) showed a fair agreement, except for some small deviations, which were most likely due to plasma intensity fluctuations during film deposition. The slight increase of the film thickness in the ion incidence angle range of 0–20° under energetic C^+ ion bombardment (Fig. 5b and c) was attributed to the dominant effect of ion implantation at small incidence

Table 1
Ion velocity change V_S due to the electric sheath at the substrate surface generated by the applied bias voltage, ion impinging angle α, and ion fluence at the substrate surface Φ_P versus ion incidence angle θ.

θ (deg.)	Substrate bias voltage (V)				Φ_P ($\times 10^{16}$ ions/cm^2)
	–25		–50		
	V_S (m/s)	α (deg.)	V_S (m/s)	α (deg.)	
0	8935	0.0	15,562	0.0	9.00
10	9026	6.6	15,689	5.3	8.86
20	9307	13.2	16,076	10.5	8.46
30	9796	19.5	16,740	15.5	7.79
40	10,530	25.4	17,708	20.1	6.89
50	11,559	30.7	19,014	24.2	5.79
60	12,951	35.3	20,700	27.6	4.50
70	14,782	38.8	22,797	30.2	3.08
80	17,116	41.0	25,322	31.8	1.56

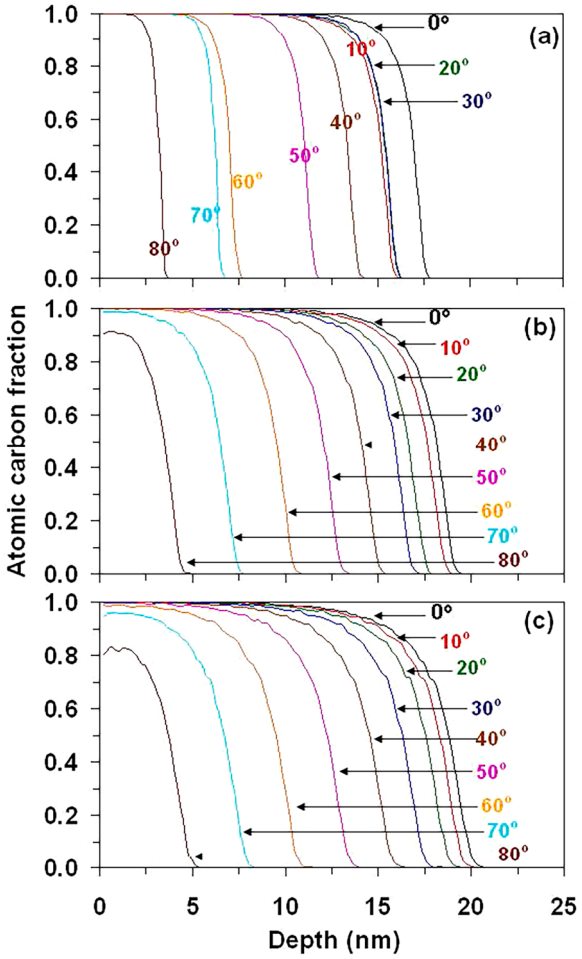

Fig. 4. Carbon depth profiles simulated with the T-DYN code for Si substrate, C^+ ion impinging angle in the range of 0–80°, and time-average substrate bias voltage equal to (a) 0 V, (b) –25 V, and (c) –50 V. The C^+ ion fluence in the plasma cloud was set equal to 9×10^{16} ions/cm^2, corresponding to 1 min film deposition in the FCVA experiments. The C^+ ion fluence at the Si surface was calculated by multiplying the ion fluence in the plasma by the cosine of the incidence angle, defined in Fig. 3. The C^+ ion fluence corresponding to each ion impinging angle is given in Table 1.

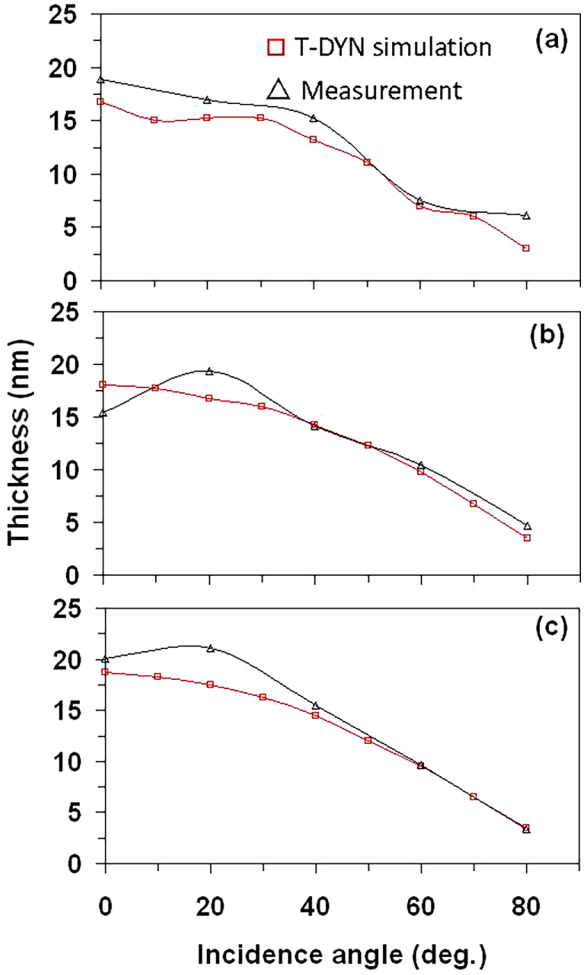

Fig. 5. T-DYN simulation results and profilometry measurements of *a*-C film thickness versus ion incidence angle for time-average substrate bias voltage equal to (a) 0 V, (b) –25 V, and (c) –50 V.

angles, whereas the decreasing trend of the film thickness in the ion incidence angle range of 20–80° was ascribed to the decrease of the ion fluence (Table 1, $\Phi_P = \Phi_I \cos\theta$) and the enhancement of ion sputter etching at high ion incidence angles. The results shown in Figs. 4 and 5 illuminate the profound effect of the ion incidence angle on the thicknesses of the intermixing layer and the *a*-C film. Additionally, since the deposition time in all FCVA experiments was fixed at 1 min, the film thickness data (Fig. 5) also represent deposition rates at different ion incident angles and substrate bias voltages.

Fig. 6 shows XPS C1s core-level peaks of *a*-C films synthesized under deposition conditions of varying ion incidence angle and substrate bias voltage. For zero substrate bias voltage, the position of the C1s peak gradually shifted to a higher binding energy with the increase of the ion incidence angle from 0 to 80° (Fig. 6a). However, for a substrate bias voltage equal to –25 V, a gradual shift of the C1s peak to a lower binding energy occurred with increasing ion incidence angle (Fig. 6b), whereas the further increase of the substrate bias voltage to –50 V did not yield a clear trend (Fig. 6c). Interestingly, for –50 V bias voltage, the C1s peak with the highest binding energy corresponded to an ion incidence angle equal to 40°. Considering the dependence of the binding energy of the C1s peak on the oxidation state and local chemical environment, affected by the adsorption of oxygen from the atmo-sphere and the carbon surface reactivity influenced by the intensity of energetic ion bombardment (substrate pulse biasing effect), the observed peak shifts may be associated with changes in the surface chemistry of the *a*-C films upon exposure to the ambient.

After performing a Shirley inelastic background subtraction [48], the XPS C1s core-level peaks were deconvoluted to extract information about the atomic carbon hybridization in each film. Details about the deconvolution methodology can be found elsewhere [46,47,49]. The carbon species in the *a*-C films exhibited sp^1, sp^2, and sp^3 hybridizations, with some high-energy surface species (referred to as the satellite peaks) attributed to physical adsorption of airborne contaminants also present in the spectra. Fig. 7 shows the fraction of each carbon component as a function of ion incidence angle and substrate bias voltage. The fraction of sp^1 hybridization was very small and constant in all *a*-C films. However, both the sp^2 and sp^3 hybridizations exhibited different trends and notable fluctuations. Specifically, while the sp^2 and sp^3 fractions varied between ~30 % and ~50 % for zero and –25 V substrate bias voltage, showing indistinguishable dependence on ion incidence angle, for –50 V substrate bias voltage, they demonstrated significantly different variations. In fact, *a*-C films with the highest sp^3 (~58 %) and lowest sp^2 (~14 %) contents were obtained for a 40° ion incidence angle. According to the subplantation model [28–30], the energetic C^+ ions penetrated up to a depth depending on the ion kinetic energy, resulting in carbon-induced densification and the development of a compressive mechanical environment, which was conducive to sp^3 hybridization. Accordingly, the enhancement of sp^3 hybridization was controlled by the intensity of

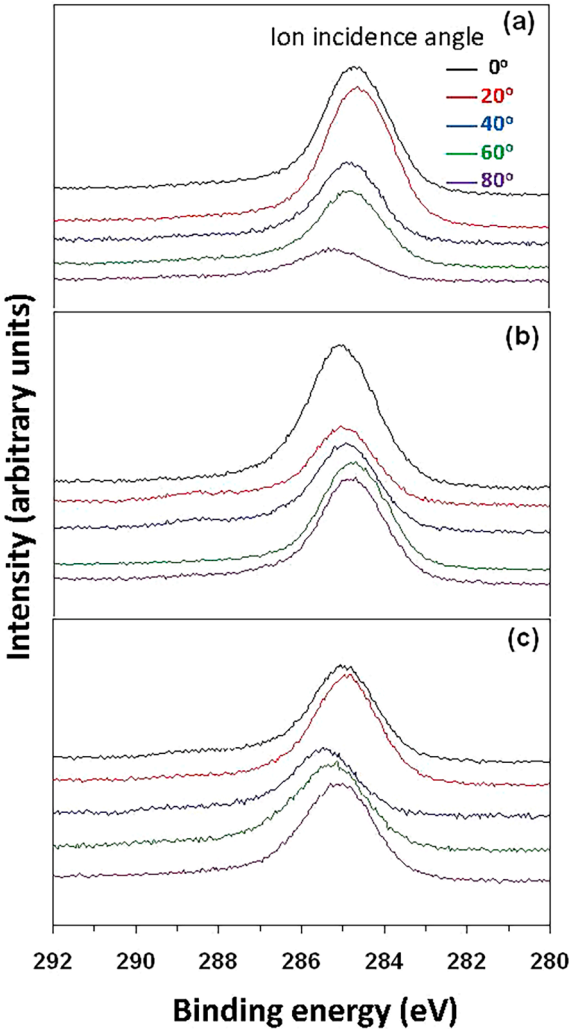

Fig. 6. XPS spectra of the C1s core-level peak of *a*-C films for ion incidence angle between 0° (normal incidence) and 80° and time-average substrate bias voltage equal to (a) 0 V, (b) –25 V, and (c) –50 V.

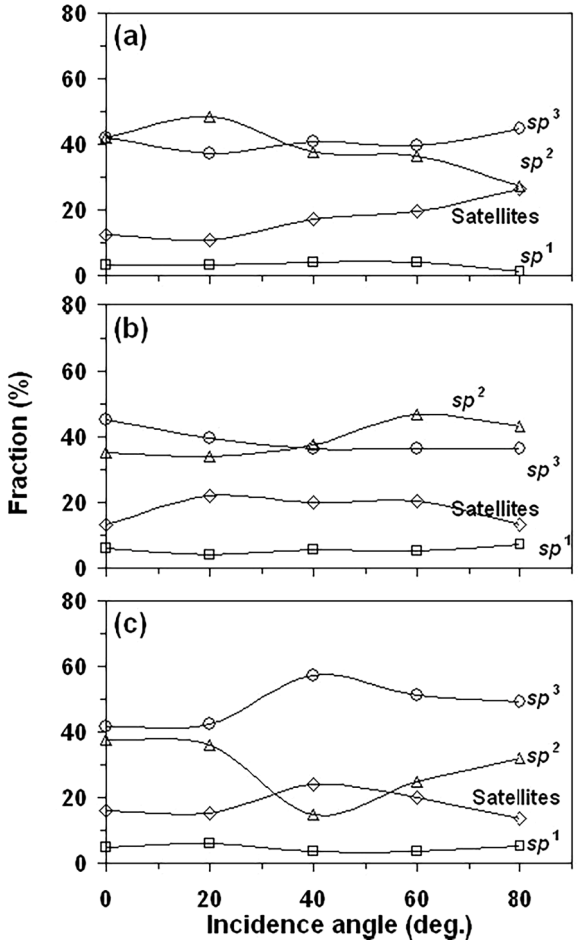

Fig. 7. Fractions of different atomic carbon hybridizations calculated from the deconvoluted C1s core-level peak of *a*-C films versus ion incidence angle for time-average substrate bias voltage equal to (a) 0 V, (b) –25 V, and (c) –50 V.

carbon-carbon collisions, which depended on the carbon concentration [50]. Consequently, because the increase of the ion incidence angle led to the decrease of the implantation depth of the impinging C^+ ions, carbon-carbon collision cascades were mostly confined within the near-surface region, contributing to the densification enhancement and the evolution of compressive stresses that favored sp^3 hybridization. However, above a critical ion incidence angle (i.e., 40°), a slight decrease of the sp^3 fraction was encountered due to the breakage of some of the sp^3 carbon bonds as a result of more intense ion bombardment, resulting in sp^3-to-sp^2 re-hybridization (Fig. 7c). Thus, the existence of a critical ion incidence angle for maximum sp^3 hybridization (i.e., 40° critical ion incidence angle for –50 V substrate bias voltage) could be attributed to lessening of the carbon-carbon collisions (decrease in carbon concentration) with the increase of the ion incidence angle.

Whereas the application of a negative substrate bias voltage intensified the ion bombardment, it also produced an ion impingement angle a smaller than the ion incidence angle θ (Table 1). This explains the slightly higher sp^3 fraction for ion incidence angles less than ~20° (Fig. 7b and c), for which the ion impinging angle was small (i.e., nearly normal ion incidence). Earlier studies showed a dependence of the sp^3 fraction of carbon films on substrate bias voltage for normal ion incidence [16,20,21]. The sp^3 fraction of carbon films having energetic C^+ ions as film precursors has been reported to increase with the magnitude of the substrate bias voltage up to about –100 V, corresponding to ~120 eV C^+ ion kinetic energy, and subsequently decrease with the increase of the bias voltage beyond –100 V [1,5,8,20,51]. Because the –25 V substrate bias voltage increased the kinetic energy of the bombarding C^+ ions only to ~45 eV, the sp^3 fraction did not change significantly with the ion incidence angle (Fig. 7b). However, increasing the substrate bias voltage to –50 V (i.e., ~70 eV ion kinetic energy) changed significantly the dependence of the sp^2 and sp^3 fractions on the ion incidence angle (Fig. 7c). Notably, the highest sp^3 fraction corresponding to 40° ion incidence angle was found to be higher than that reported for higher (–100 V) substrate bias voltage, but zero ion incidence angle [16,43]. This difference in sp^3 fraction may be related to the development of a more compressive mechanical environment due to the increased carbon concentration at the surface under oblique ion incidence, which intensified carbon-carbon collision cascades that favored sp^3 hybridization. Even though the sp^3 fraction decreased slightly in the depositions with ion incidence angles greater than 40° and –50 V substrate bias voltage, it remained much higher than the sp^2 fraction. Whereas the predominance of sp^3 hybridization may also be attributed to preferential sputtering of the sp^2 hybridized carbon domains, this conjecture was not supported by the analysis of the T-DYN simulation results, which showed negligible sputtering yield (Fig. 8a) and backscattering (Fig. 8b) under the present deposition conditions. A more likely supposition is that oblique incidence of the energetic C^+ ions activated atomic collisions at the growing film surface, transferring energy that increased the momentum of surface atoms, consecutively enhancing sp^3 hybridization, as opposed to perpendicularly impinging ions that were implanted deeper into the substrate. Indeed, results of the mean projected range (Fig. 8c) showed a

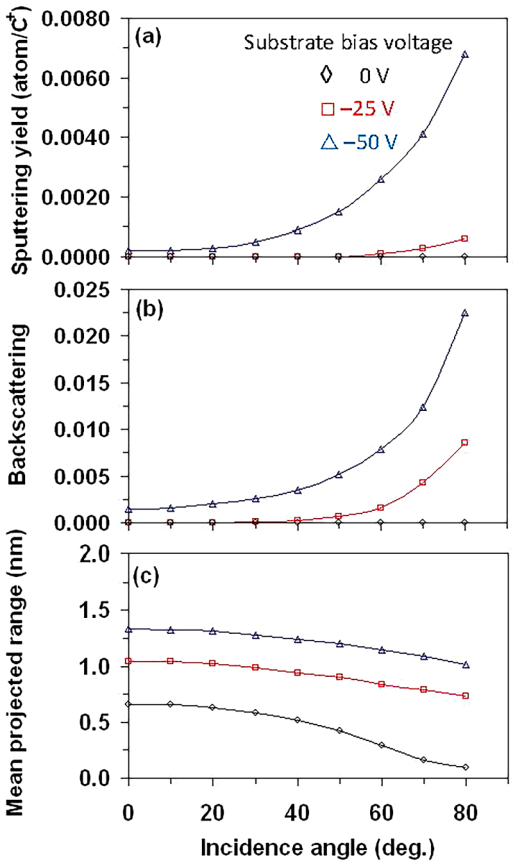

Fig. 8. T-DYN simulation results of (a) sputtering yield, (b) backscattering, and (c) mean projected range for C^+ ions impinging onto a Si surface versus ion incidence angle and time-average substrate bias voltage equal to 0, –25, and –50 V.

decrease in ion travel distance with increasing ion incidence angle, suggesting that carbon-carbon atom collisions and film densification were confined at the outermost surface region of the film. Thus, the decrease of the ion fluence with the increase of the ion incidence angle (Table 1) was compensated by the confinement of carbon atom collisions within the near-surface region of the growing film, which promoted sp^3 hybridization. Consequently, the high sp^3 content can be ascribed to the enhancement of surface atom collision cascades, with optimum conditions encountered under FCVA conditions of 40° ion incidence angle and –50 V substrate bias voltage.

In addition to the ion incidence angle effect on the thickness and structure of the FCVA-deposited *a*-C films, the resulting surface roughness is also of high importance in applications requiring ultrasmooth surfaces, such as microelectronics, photonics, and magnetic recording technologies. Fig. 9 shows the dependence of the *a*-C film roughness on the ion incidence angle for various substrate bias voltages. The slight surface roughening caused by the increase of the ion incidence angle observed in all depositions can be associated with the intensification of resputtering under oblique ion bombardment. This conjecture is supported by the decrease of the film thickness with increasing ion incidence angle (Fig. 5). The somewhat smoother films synthesized under a substrate bias voltage of –25 V may be related to less atomic displacement in these films compared to the films deposited under a substrate bias voltage of –50 V. Comparatively less sp^3 hybridization and higher surface roughness was observed in previous studies [30,46]. This suggests that the smoother *a*-C films synthesized under conditions of 40° ion incidence angle and –50 V substrate bias voltage may be correlated with the high sp^3 fraction of these films (Fig. 7c), attributed to the compressive mechanical environment at the growing film surface produced under oblique ion incidence deposition conditions.

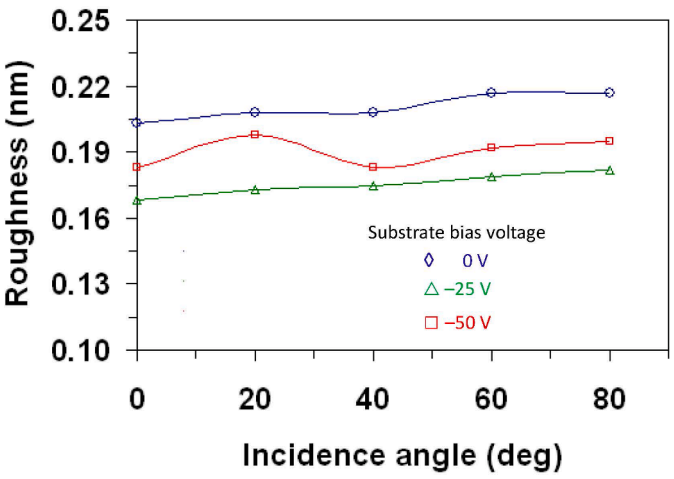

Fig. 9. Variation of rms surface roughness of *a*-C films with ion incidence angle for time-average substrate bias voltage equal to 0, –25, and –50 V.

4. Conclusions

The thickness, structure, and roughness of nanometer-thick *a*-C films deposited by the FCVA technique for ion incidence angles in the range of 0–80° and time-average substrate pulse bias voltage of magnitude equal to 0, –25, and –50 V were characterized in the light of T-DYN simulation results and XPS, surface profilometry, and AFM measurements. Carbon film growth, sp^3 hybridization, and surface texturing at oblique ion incidence were interpreted in the context of simulation and experimental results. The C^+ ion fluence on the substrate surface decreased with the increase of the ion incidence angle, consequently leading to deposition of thinner films. Carbon atom hybridization was also affected by the ion incidence angle and applied substrate bias voltage. *a*-C films with the highest sp^3 fraction (~58 %) were deposited under FCVA plasma conditions of 40° ion incidence angle and –50 V substrate bias voltage. The increase of the sp^3 hybridization was attributed to carbon-carbon atomic collisions at the growing film surface and the densification induced by direct and recoil implantation processes controlled by the ion incidence angle and substrate bias voltage. The marginal increase of the surface roughness of the *a*-C films with the ion incidence angle was correlated with the enhancement of sputter etching under oblique ion incidence. The simulation-experimental approach presented in this study provides a ground base for further investigations aimed to optimize the ion incidence angle for depositing smooth, highly sp^3 hybridized carbon thin films under various substrate bias voltages.

CRediT authorship contribution statement

Hanshen Zhang: Conceptualization, Writing – original draft. **Kyriakos Komvopoulos:** Supervision, Writing – review & editing, Resources.

Declaration of Competing Interest

The authors declare no competing interests.

Data availability

Data will be made available on request.

References

[1] J. Robertson, Ultrathin carbon coatings for magnetic storage technology, Thin Solid Films 383 (2001) 81–88.
[2] J. Robertson, Diamond-like amorphous carbon, Mater. Sci. Eng. R. Rep. 37 (2002) 129–281.
[3] T. Yamamoto, H. Hyodo, Amorphous carbon overcoat for thin-film disk, Tribol. Int. 36 (2003) 483–487.
[4] A. Roy, S. Wang, K. Komvopoulos, A review of plasma-assisted deposition methods for amorphous carbon thin and ultrathin films with a focus on the cathodic vacuum arc technique, J. Mater. Res. 38 (2023) 586–616.
[5] S. Anders, A. Anders, I.G. Brown, B. Wei, K. Komvopoulos, J.W. Ager III, K.M. Yu, Effect of vacuum arc deposition parameters on the properties of amorphous carbon thin films, Surf. Coat. Technol. 68-69 (1994) 388–393.
[6] H. Han, F. Ryan, M. McClure, Ultra-thin tetrahedral amorphous carbon film as slider overcoat for high areal density magnetic recording, Surf. Coat. Technol. 120-121 (1999) 579–584.
[7] P.R. Goglia, J. Berkowitz, J. Hoehn, A. Xidis, L. Stover, Diamond-like carbon applications in high density hard disc recording heads, Diam. Relat. Mater. 10 (2001) 271–277.
[8] E. Byon, A. Anders, Ion energy distribution functions of vacuum arc plasmas, J. Appl. Phys. 93 (2003) 1899–1906.
[9] B.F. Coll, P. Sathrum, R. Aharonov, M.A. Tamor, Diamond-like carbon films synthesized by cathodic arc evaporation, Thin Solid Films 209 (1992) 165–173.
[10] A. Anders, Metal plasma immersion ion implantation and deposition: a review, Surf. Coat. Technol. 93 (1997) 158–167.
[11] B. Schultrich, H.-J. Scheibe, D. Drescher, H. Ziegele, Deposition of superhard amorphous carbon films by pulsed vacuum arc deposition, Surf. Coat. Technol. 98 (1998) 1097–1101.
[12] A. Anders, Approaches to rid cathodic arc plasmas of macro- and nanoparticles: a review, Surf. Coat. Technol. 120-121 (1999) 319–330.
[13] A. Anders, R.A. MacGill, Twist filter for the removal of macroparticles from cathodic arc plasmas, Surf. Coat. Technol. 133-134 (2000) 96–100.
[14] G.F. You, B.K. Tay, S.P. Lau, D.H.C. Chua, W.I. Milne, Carbon arc plasma transport through different off-plane double bend filters, Surf. Coat. Technol. 150 (2002) 50–56.
[15] B. Petereit, P. Siemroth, H.-H. Schneider, H. Hilgers, High current filtered arc deposition for ultra thin carbon overcoats on magnetic hard disks and read-write heads, Surf. Coat. Technol. 174-175 (2003) 648–650.
[16] H.-S. Zhang, K. Komvopoulos, Direct-current cathodic vacuum arc system with magnetic-field mechanism for plasma stabilization, Rev. Sci. Instrum. 79 (2008), 073905.
[17] J. Xie, K. Komvopoulos, Thermal stability of ultrathin amorphous carbon films synthesized by plasma-enhanced chemical vapor deposition and filtered cathodic vacuum arc, Philo. Mag. 97 (2017) 820–832.
[18] N. Wang, K. Komvopoulos, Thermal stability of ultrathin amorphous carbon films for energy-assisted magnetic recording, IEEE Trans. Magn. 47 (2011) 2277–2282.
[19] S. Wang, A. Roy, K. Komvopoulos, Thermal stability and diffusion characteristics of ultrathin amorphous carbon films grown on crystalline and nitrogenated silicon substrates by filtered cathodic vacuum arc deposition, Sci. Rep. 11 (2021) 13106.
[20] G.M. Pharr, D.L. Callahan, S.D. McAdams, T.Y. Tsui, S. Anders, A. Anders, J. W. Ager III, I.G. Brown, C.S. Bhatia, S.R.P. Silva, J. Robertson, Hardness, elastic modulus, and structure of very hard carbon films produced by cathodic-arc deposition with substrate pulse biasing, Appl. Phys. Lett. 68 (1996) 779–781.
[21] T.A. Friedmann, J.P. Sullivan, J.A. Knapp, D.R. Tallant, D.M. Follstaedt, D. L. Medlin, P.B. Mirkarimi, Thick stress-free amorphous-tetrahedral carbon films with hardness near that of diamond, Appl. Phys. Lett. 71 (1997) 3820–3822.
[22] J. Matlak, K. Komvopoulos, Friction properties of amorphous carbon ultrathin films deposited by filtered cathodic vacuum arc and radio-frequency sputtering, Thin Solid Films 579 (2015) 167–173.
[23] B.K. Pathem, X.-C. Guo, F. Rose, N. Wang, K. Komvopoulos, E. Schreck, B. Marchon, Carbon overcoat oxidation in heat-assisted magnetic recording, IEEE Trans. Magn. 49 (2013) 3721–3724.
[24] S. Wang, K. Komvopoulos, A molecular dynamics study of the oxidation mechanism, nanostructure evolution, and friction characteristics of ultrathin amorphous carbon films in vacuum and oxygen atmosphere, Sci. Rep. 11 (2021) 3914.
[25] J. Matlak, K. Komvopoulos, Ultrathin amorphous carbon films synthesized by filtered cathodic vacuum arc used as protective overcoats of heat-assisted magnetic recording heads, Sci. Rep. 8 (2018) 9647.
[26] J. Xie, K. Komvopoulos, The role of duty cycle of substrate pulse biasing in filtered cathodic vacuum arc deposition of amorphous carbon films, IEEE Trans. Magn. 51 (2015), 3302009.
[27] N. Wang, K. Komvopoulos, The effect of deposition energy of energetic atoms on the growth and structure of ultrathin amorphous carbon films studied by molecular dynamics simulations, J. Phys. D 47 (2014), 245303.
[28] Y. Lifshitz, S.R. Kasi, J.W. Rabalais, W. Eckstein, Subplantation model for film growth from hyperthermal species, Phys. Rev. B 41 (1990) 10468–10480.
[29] Y. Lifshitz, C.D. Roux, K. Boyd, W. Eckstein, J.W. Rabalais, Analysis of carbon film growth from low energy ion beams using dynamic trajectory simulations and Auger electron spectroscopy, Nucl. Instrum. Methods Phys. Res. B 83 (1993) 351–356.
[30] Y. Lifshitz, G.D. Lempert, E. Grossman, Substantiation of subplantation model for diamondlike film growth by atomic force microscopy, Phys. Rev. Lett. 72 (1994) 2753–2756.
[31] S. Wang, K. Komvopoulos, Structure evolution during deposition and thermal annealing of amorphous carbon ultrathin films investigated by molecular dynamics simulations, Sci. Rep. 10 (2020) 8089.
[32] N. Wang, K. Komvopoulos, The multilayered structure of ultrathin amorphous carbon films synthesized by filtered cathodic vacuum arc deposition, J. Mater. Res. 28 (2013) 2124–2131.
[33] J. Xie, K. Komvopoulos, Bilayer amorphous carbon films synthesized by filtered cathodic vacuum arc deposition, J. Mater. Res. 31 (2016) 3161–3167.
[34] H.-S. Zhang, K. Komvopoulos, Scale-dependent nanomechanical behavior and anisotropic friction of nanotextured silicon surfaces, J. Mater. Res. 24 (2009) 3038–3043.
[35] K.-H. Müller, Role of incident kinetic energy of adatoms in thin film growth, Surf. Sci. 184 (1987) L375–L382.
[36] M.T. Robinson, I.M. Torrens, Computer simulation of atomic-displacement cascades in solids in the binary-collision approximation, Phys. Rev. B 9 (1974) 5008–5024.
[37] O.S. Oen, D.K. Holmes, M.T. Robinson, Ranges of energetic atoms in solids, J. Appl. Phys. 34 (1963) 302–312.
[38] M.T. Robinson, O.S. Oen, Computer studies of the slowing down of energetic atoms in crystals, Phys. Rev. 132 (1963) 2385–2398.
[39] W.D. Wilson, L.G. Haggmark, J.P. Biersack, Calculations of nuclear stopping, ranges, and straggling in the low-energy region, Phys. Rev. B 15 (1977) 2458–2468.
[40] J. Lindhard, M. Scharff, Energy dissipation by ions in the kev region, Phys. Rev. 124 (1961) 128–130.
[41] J. Biersack, TRIM-DYNAMIC applied to marker broadening and SIMS depth profiling, Nucl. Instrum. Methods Phys. Res. B 153 (1999) 398–409.
[42] R. Kosiba, G. Ecke, MC simulations of depth profiling by low energy ions, Nucl. Instrum. Methods Phys. Res. B 187 (2002) 36–47.
[43] H.-S. Zhang, K. Komvopoulos, Synthesis of ultrathin carbon films by direct current filtered cathodic vacuum arc, J. Appl. Phys. 105 (2009), 083305.
[44] G. Ecke, R. Kosiba, V. Kharlamov, Y. Trushin, J. Pezoldt, The estimation of sputtering yields for SiC and Si, Nucl. Instrum. Methods Phys. Res. B 196 (2002) 39–50.
[45] R.M. Hausner, H. Baumann, K. Bethge, Aluminum ion implantation under backfilling oxygen, Nucl. Instrum. Methods Phys. Res. B 113 (1996) 176–181.
[46] H.-S. Zhang, J.L. Endrino, A. Anders, Comparative surface and nano-tribological characteristics of nanocomposite diamond-like carbon thin films doped by silver, Appl. Surf. Sci. 255 (2008) 2551–2556.
[47] D. Wan, K. Komvopoulos, Tetrahedral and trigonal carbon atom hybridization in thin amorphous carbon films synthesized by radio-frequency sputtering, J. Phys. Chem. C 111 (2007) 9891–9896.
[48] D.A. Shirley, High-resolution X-ray photoemission spectrum of the valence bands of gold, Phys. Rev. B 5 (1972) 4709–4714.
[49] W. Lu, K. Komvopoulos, S.W. Yeh, Stability of ultrathin amorphous carbon films deposited on smooth silicon substrates by radio frequency sputtering, J. Appl. Phys. 89 (2001) 2422–2433.
[50] D. Wan, K. Komvopoulos, Probabilistic analysis of tetrahedral carbon hybridization in amorphous carbon films, Appl. Phys. Lett. 88 (2006), 221908.
[51] V.S. Veerasamy, G.A.J. Amaratunga, W.I. Milne, J. Robertson, P.J. Fallon, Influence of carbon ion energy on properties of highly tetrahedral diamond-like carbon, J. Non-Cryst. Solids 164–166 (1993) 1111–1114.